# Interpretation of Deformation Pattern in Automotive Rails in Frontal Impact

**Joseph Hassan, K. Ding and G. Nusholtz**
Scientific Labs and Proving Grounds DaimlerChrysler Corp. USA

## ABSTRACT

Two barriers are commonly used to evaluate the response of a vehicle in a frontal impact: the rigid barrier and the offset deformable barrier. They produce different deformation patterns, which opens up the possibility that at least one of them does not represent real world crashes. One possible cause of the difference is that an impact into a rigid barrier generates significantly greater stress waves than impacts in the real world resulting in final deformation patterns that are different from those seen in the field. To evaluate this conjecture models of two types of rails each undergoing two different types of impacts, are analyzed using an explicit dynamic finite element code. Results show that the energy perturbation along the rail depends on the barrier type and that the early phase of wave propagation has very little effect on the final deformation pattern. This implies that in the real world conditions, the stress wave propagation along the rail has very little effect on the final deformed shape of the rail.

## INTRODUCTION

In any vehicle impact simulation, the deformation of certain components or substructures are of special interest. For instance during frontal barrier impact, the forestructure forward of the passenger compartment deforms plastically, while that behind remains essentially undeformed. Consequently, the front-end structure experiences large deformations in the order of 500 ~ 800 mm in a time interval of 100 ~ 140 msec in a vehicle to vehicle impact and 60 to 90 msec in vehicle to barrier crash. In such an event, structural members that are subjected to inertia and reaction forces beyond their ultimate load collapse first. In a typical front end crash for a front wheel drive vehicle, a significant amount of the plastic energy is absorbed by the rails in the form of plastic strain energy [1,2]. In this process, the deformation pattern of the rail corresponds to the areas where stresses exceed its yield limit.

The final deformation of the rail has been found to be dependent upon the barrier type that is interacting with the vehicle [1,2]. Several factors may be considered the cause of these different final deformations. One such factor may be the contact forces between the barrier and the rail. Several studies however, point out that in any structural impact event, energy of the impact is transmitted in the form of stress waves that initiate at the impact end and propagate through the media to other points on the structure [6]. These stress waves propagating during the early phases of impact may determine the deformation pattern of the latter part of the event.

In an attempt to gain insight into the effect of the stress waves propagating in the early part of an impact event on the response of a vehicle rail, an analytical approach is presented based on the finite element method. In this study models of two types of rails each undergoing two different types of impacts (deformable and rigid), are analyzed. To accentuate the effect of wave propagation along the rail, all vehicle components that are normally between the rail and the barrier are removed from the model. Thus the rail models are put in direct contact with the barrier. Therefore, if there is any effect present due to stress waves on rail's final deformation, it will manifest itself in the response. However, if no effect is found, the implication is that in the real world conditions, the stress wave propagation along the rail has very little effect on the final deformed shape of the rail in a barrier impact. Towards that end, the effect of the stresses and the internal energy at different locations occurring early in the event as it affects the response at later stages is computed and reported here.

## COMPUTER BASED MODEL

Towards the above objective, finite element models of two rails (figures 1,2) are used in this investigation. One model is for a straight rail with stress risers that act as buckling initiators at specific locations,

referred to as "type -1" and the other is for a curved rail, referred to as "type-2". In addition a model was used to simulate a deformable barrier. The models are used to perform transient, dynamic, nonlinear impact analysis of the rail system, utilizing an explicit code. The models were extracted from full vehicle models subjected to the same impact conditions and validated against experimental tests [3,4]. The models were given an initial velocity of 30 mph toward a rigid barrier or a deformable barrier. Each of the models is considered to be of adequate fidelity to completely cover the major geometry and the targeted analysis areas.

Shell elements are used for the rails and part of the deformable barrier. Solid elements are primarily used to model the deformable barrier. Both type-1 and type-2 rails comprised of shells and rigid bodies. The shells are modeled with plastic material of LSDYNA type 3 or 24. Strain rate effect is not accounted for in this analysis. LSDYNA Ver 950c is used to analyze the response. Initial and applied conditions are extracted from the full model and applied to the components model. Both rails are used to simulate full frontal impact.

## PROPOSED METHODOLOGY

A time history based comparison is made between the characteristic behavior of each rail in a deformable barrier and rigid barrier. Some crash analysts use static analysis to evaluate vehicle crash. The static crush, a phenomenon that is independent of time, does not exhibit stress wave propagation. Therefore, further comparison is made between the initial deformation pattern under rigid and deformable barrier impacts and static crush. The static case is computed by assuming that the axial rail deformation obtained in the dynamic analysis is maintained the same as in the static crush, for each time frame considered. For example if we are to compare the dynamic behavior of the rail at 1 msec, the rail total crush distance at 1 msec say 10 cm, is used as the input for the total displacement of the rail in the static analysis. To compare the wave propagation effect along the rail, each rail was divided into a number of regions of equal length as shown in figures 1 and 2.

To address the robustness of this approach, the effect of the variable nature of the rail geometry and composition on the resulting wave propagation and its effect was also analyzed. The internal energy density is computed for type-1 rail with different thickness and density for both rigid and deformable impacts. Towards that end, type-1 rail was divided into four equal sections and the energy density was computed for each section. Variability in rail thickness and density was examined by varying each section's thickness or density with respect to the rest of the rail. In each case the thickness or density of one of the sections was doubled with respect to the rest of the rail. Internal energy density was computed in each case and compared to the baseline for both rigid and deformable impacts. Table –1 summarizes the cases analyzed and reported in this paper.

Table-1 Summary of cases analyzed

| Rail geometry | Deformable Barrier | Rigid Barrier | Static crush |
|---|---|---|---|
| Type -1 | Initial and Final phases | Initial and Final phases | Final deformation |
| Type -2 | Initial phase of impact | Initial phase of impact | Final deformation |

## RESULTS AND DISCUSSION:

To compare the effect of deformable barrier and rigid barrier on different types of rails, results are examined in the form of rail load carrying capacity, deformation (crash) pattern and stress wave propagation phenomena. The stress wave propagation is analyzed in terms of stress, deformation patterns and plastic strain energy. Robustness of the technique is examined in terms of the effect of varying density and thickness on the energy aspect of wave propagation.

## RAIL LOADING CHARACTERSITICS:

Load carrying capacity in the form of barrier contact forces is shown in figure 7 and 8. The load at a cross section located close to the barrier (specifically at the third raw of elements parallel to the barrier face) is computed for both rails. Comparative results indicate that the maximum load as a result of rigid impact is much higher than in the deformable impact. This result is also enforced by examining figure 9 and 10 where the plastic strain at different locations along the rail is much higher in the rigid barrier case than in the deformable case.

## STRESS WAVE PROPAGATION EFFECT

Because of it's complexity, the complete understanding of stress wave propagation in vehicle rails is beyond the scope of this paper; however, by looking at two types of significantly different rails interacting with two types of barriers, a general understanding of the impact response should be obtained. For the purpose of describing the complexity and elaborating on why a simple model of a rail may not give adequate insights a description of some of the possible mechanics is described in what follows.

A typical rail response in an impact with a barrier, in it's initial phase, can be characterized as a form of stress wave propagation phenomenon. The mathematical formulation of this problem can be given by a system of hyperbolic differential equations. The classical solution for simplified cases of this phenomenon is described in a number of publications including [5,6]. A time history response takes the form of waves originating at the impact end and traveling away in the rail. Depending on the type of wave propagating, stresses and energy travels away from the impact end at different speeds. In solid media such as the rail, incident dilatation waves are propagated down the rail in the form of compressive stresses away from the barrier end. The speed of the dilatation waves is dependent upon the material properties and can be found in the literature [6,7]. These waves are reflected at boundaries of changes in material properties, geometrical discontinuities and loading conditions. Fixed boundaries such as rigid barriers, cause reflected wave that is of the same type as the incident wave. Therefore, at a rigid barrier a dilatation compressive wave is reflected as a dilatation compressive wave. Completely "free" boundaries cause reflected waves that are of opposite sign to the incident waves. Thus a compressive wave is reflected as tension wave. However, in the deformable barrier case, upon impact, two families of waves will be generated, one family propagating into the rail and the other into the barrier. Depending on the initial values at the interface and the material properties of both sides of the interface, compressive dilatation stress waves are reflected at the impact end in both the rail and the barrier. The strain at both sides of the interface is not equal therefore, the magnitude of the reflected dilatation wave is a fraction of the incident wave but of the same compressive type. A full explanation of the reflection at soft interfaces is given in [8].

To quantify the stress and crash pattern during early phases of barrier impact, the first peak stress wave was tracked along the rail. Successive stress patterns in the form of plastic strain measures can be plotted at different rail locations as described in figure 1 and 2, at different points in time. A quantitative assessment for the wave propagation can be followed along each rail in specific locations. Plots of plastic strain history along rail length at different locations are used to present the effect at different times of the early phase of the crash. Figure 9 depicts a typical behavior for type-1 rail for the rigid barrier, while figure 10 represents the behavior for deformable barrier. It can be seen from the analysis that the speed of the elastic dilatation wave in both cases of impact is 5.10e+06 mm/sec which agrees with the known value for steel.

Figures 11 and 12 depict stress wave propagation in type 1 and type 2 rails in both deformable barrier, rigid barrier impacts. In addition the figures contain the results from an equivalent static crush case that is based on the same amount of rail reduction for each time increment presented (i.e. at 0.05, 0.1, 0.15 and 0.2 msec). The figures point out the following:

1. In the dynamic impacts stress waves propagate from the impacted end. This is apparent from observing the plastic deformation zone as it traverses the full length of the rail in approximately 0.2 msec.

2. The distributions of the yield stresses in the dynamic impacts are time and geometry dependent; whereas, the static crush is only geometrically dependent. For example, in the dynamic impact, in the first 0.05 msec areas of yield are only in the first quarter of the length of the rail; whereas, in the static crush the yield can occur in any location throughout the rail depending on the geometry. In the following 0.05 msec for the dynamic impacts the yielded area progresses another quarter of the length.

3. Major variations in the stress contours exist once the wave encounters a drastic change in geometry such as holes, slots etc. The propagation of the plastic zones has much higher plastic stress when approaching a geometrical hole boundary than when it departs

4. The magnitude of the plastic stress in the areas where yield has occurred are higher in the dynamic impacts than in the static crush before 0.2 msec. It will be comparatively higher earlier in the event and become similar as time evolves.

5. For the same crush distance, dynamic impact has less plastic zone than in static crush. While in the static case there are regions of plastic stress present in 100 % of the rail, it is only limited to 10% of the rail in the neighborhood of the impact point in the dynamic case.

## STRESS WAVES RESULTS (Type-1 Rail)

Figure 11 represents the deformation pattern for type-1 rail. The figure depicts a comparison between the rigid wall, deformable barrier and static crush effects in the early phase of wave propagation (up to 1 wave travel). The mechanism by which each impact propagates can be described as follows;

### A- RIGID BARRIER IMPACT:

- At 0.05 msec the yielded area extends up to ¼ of the rail. It further extends to about ½ the rails length after 0.1 msec. Minor variations in the stress contours exist once the wave encounters a drastic change in geometry such holes, slots etc. The wave then propagates to ¾ of the rails length at 0.15 msec and cover the full rail length after 0.2 msec.
- Visible deformation occurs near the holes in the rail approximately one-third the distance of the rail from the impacted end in the first 0.1 msec. In addition, the dynamic plastic deformation, while detectable is not significantly different than in the static crush.

### B- DEFORMABLE DYNAMIC IMPACT

- At first contact between the rail and the deformable barrier, there is a compressive wave propagates down the rail. But there is also a wave propagates in the opposite direction in the barrier material.
- At 0.05 msec the yielded area extends up to ¼ of the rail, however at 0.1 and 0.15 msec the fringes indicate that the elastic-plastic zone does not extend any further than the first ¼ . However, plastic zones reappear again at 0.2 msec further down the rail with a discontinuous stress pattern. In addition, the plastic deformation after 0.2 msec has very little detectable difference from the static crush.

## STRESS WAVES RESULTS (Type-2 Rail)

Figure 12 represents the deformation pattern for this case. The figure depicts a comparison between the rigid wall, deformable barrier and static crush effect in the early phase of the wave propagation (up to 2 wave lengths). The mechanism by which each impact propagates can be explained as follows;

### A- CHARACTERISTICS OF RIGID DYNAMICS OF TYPE-2 RAIL

- At 0.05 msec the yielded area extends more than ¼ of the rail. The zone also extends to more than ½ length at 0.1 msec. However upon reaching mid point, the deeply curved shape acts as a global stress concentration agent. Thus the stress pattern changes. The highest stress occurs at the corner of the curved shape once the wave arrives at that discontinuity.

- At 0.2 msec, the elastic-plastic zone extends the total length of the rail but with major discontinuity at the outer edges. However, the plastic deformation after 0.2 msec has very little detectable difference from the static crush.

## B- CHARACTERISTICS OF DEFORMABLE DYNAMICS OF TYPE-2 RAIL

- Stress wave originated at the impact end propagates down the rail to cover more than ¼ the rail's length after 0.05 msec as the case with rigid barrier. It extends to more than ½ length after 0.1 msec. However, once the wave encounters the curved shape of the rail, it shows different stress pattern that can be described as discontinuous at the outer edges of the rail.
- At 0.2 msec the compressive stress changes from large cluster to scattered areas along the rail.
- The curved corner acts as a global stress concentration agent. The highest stress occurs at the corner of the curved shape. This is similar to the rigid barrier case. However, the plastic deformation after 0.2 msec has very little detectable difference from the static crush.

## GENERAL DISCUSSION ON STRESS WAVES EFFECT:

- The propagation of the plastic zones has much higher plastic stress when approaching a geometrical hole boundary than when it departs. This suggests that the hole has a strengthening effect when the wave is approaching (very similar to the static case), but reflection of the waves around the hole has the opposite influence on the magnitude of the stress since the values of the stress are much lower than the one approaching the hole.
- In the static case, stress distribution along the rail complies with the stress flow pattern that exists in the media, rather than wave propagation pattern. The flow pattern formulation follows an Airy stress function type such as described in the classical formulation presented in [7].
- In some rail geometry (such as type –2), the geometrical stress concentration is of such a massive contribution even in the dynamic cases, that the effect of wave propagation becomes negligible. In such a case the total deformation complies with the stress flow pattern that exists in the media, rather than wave propagation pattern very similar to the behavior in the static case.
- For type-1 rail in the case of the rigid barrier, the crash zone increases with wave propagation as evidenced by (figure 11) and stress wave plots at 1,2,3,4 msec (figure 9). However, for the deformable barrier case (figure 11), at different times the stress propagation does not change significantly, therefore, the contours and stress wave plots (figure 9) at 1,2,3,4 msec are similar. This early phase of wave propagation has very little effect on the final deformation (crush) pattern since the full duration of the impact is of several thousands wave reflections and refraction. This can be seen from comparison between the final deformation pattern for type-1 rail under rigid impact, deformable barrier impact and static crush, as shown in figures 3,5 and 5B. The figures show very little difference between all three cases. This implies that in the real world conditions, the stress wave propagation along the rail has very little effect on the final deformed shape of the rail in a barrier impact

- For the Type-2 rail in both rigid and deformable impacts, there is a direct correlation between the extent of the crash zone and the wave propagation; crash zone increases as wave propagates. But the stress increases more vigorously at the rigid barrier impact than that at the deformable barrier impact. Due to the existence of a deeply curved shape somewhere in the middle of the rail, it acts as a global stress concentration for all propagating waves as well as for the static case. Therefore deformation the pattern for this rail is found to more or less common in all three cases. However, results of figures 4 and 6 also show that this early phase of wave propagation has very little effect on the final deformation (crush) pattern since the full duration of the impact is of several thousands wave reflections and refraction. This implies that in the real world conditions, the stress wave propagation along the rail has very little effect on the final deformed shape of the rail in a barrier impact.

The results of stress wave propagation effect can be summarized in table-2 for different cases considered.

Table –2 Effect of stress waves on final deformation

| Rail analyzed | Deformable Barrier | Rigid Barrier |
|---|---|---|
| Type -1 | Not Significant nor detectable | Not Significant but detectable |
| Type -2 | Not Significant nor detectable | Not Significant nor detectable |

## Effect of wave propagation on internal energy:

The different deformation patterns of type-1 and type-2 rails for rigid and deformable impacts are analyzed with the aid of the internal energy density. This quantity is evaluated for different sections of the rail. Loc. 1 and Loc. 4 are at the end points of the rail, while Loc.2 is about 40% of the length away from Loc. 1 and Loc. 3 is about 80% of the length away from Loc. 1. For type –1 rail, as shown in Figure 13, the internal energy density at Loc. 1, which is closest to the barriers is higher than that at the other three locations for both barrier impacts as shown in figures 13-a and 13-c. This reflects the notion that high deformation occurs at the impact end regardless of barrier type. However, the internal energy density in the rigid case at Loc. 1 is higher than that in the deformable case. The severity of the impact can be estimated by examining the perturbation of the internal energy along the rail. This can be done by computing the perturbation order of the energy density at each location. The perturbation order of this quantity at the other three locations as shown in figures 13-b and 13-d, is found to be different between the two barrier cases. It can be seen from the figures that Loc. 3 is the second highest density followed by Loc. 2 and then Loc. 4 for the rigid case, but it is Loc. 4, 3 and 2 for the deformable case. This can be interrupted as being due to the different type of the waves propagating at different times. In addition it appears that the rigid case generates more plastic energy and deformation concentrated near the impact end.

For type-2 rail, as shown in Figure 14, the internal energy density at Loc. 1 for the rigid case and Loc. 4 for the deformable case are higher than that of the other three locations. The energy perturbation order of at these locations is also different. They are Loc. 3, 4 and 2 for the rigid case and Loc. 2, 3 and 1 for the deformable case. However, since it was found that the stress waves propagation has very little effect on the final deformation pattern, it follows that the energy perturbation order has very little effect on the final deformation pattern of the rails considered in this investigation.

## Effect of thickness and density variability on wave propagation:

In order to address the robustness of this approach, the effect of the variable nature of the rail geometry and composition was analyzed**.** The same four sections of the rails as described above are used for this analysis. Loc. 1 to Loc. 4 represent the four locations from the barrier end to the other end of the rail respectively. The internal energy density time history are given in Figure 15 for the rigid case and Figure 16 for the deformable case where the thickness of one portion of type-1 rail is doubled with respect to the nominal baseline thickness. A comparison can be made between the case where the rail thickness is constant as shown in Figure 16A for the rigid case and Figure 16B for the deformable case, for both impact cases, the magnitude of energy at Loc. 1 drops drastically if the thickness in any portion is increased. The internal energy density at the other three locations are not quite affected by the change of the thickness, except for Loc. 2 of the rail at rigid impact. The increase of the thickness at the front and the rear portion significantly changes the internal energy density.

Figures 17A to 18D are the counterpart for the density analysis. The doubling of the density effectively drops the internal energy density of Loc. 1 as thickness increases. However, in this case Loc. 4 is the one at which the internal energy density changes significantly as the density at the rear portion is increased.

The density change results in the descending order of the internal energy density being Loc. 4, 3, 1 and 2 as the portions other than Loc.1 doubles its density; while the rail with constant density has the order of Loc. 1, 4, 3 and 2. Although the doubling of the front portion density does not alter the order of Loc. 1, 4, 3 and 2, the figures show that the density alters the deformation pattern more significantly than the thickness change. This may be understandable

since changes in thickness affect only the mass and stiffness of the component while changes in density affect not only mass and stiffness but also speed of wave propagation.

In the above cases changing the density or thickness changed the deformation pattern; none the less, the same trend as seen in the unaltered rails was observed--the effect of stress waves on the final deformation was negligible. In other words changes to the rails that affect the final deformation do not change the effect of stress waves on that final deformation.

## GENERAL CONCLUSIONS:

Comparative results of type-1 rail and type-2 rail indicate that the load on the cross section of both rails as the result of rigid impact is much higher than the maximum load in the deformable impact.

It seems that the effect of stress wave propagation at early stage of impact is dependent upon the barrier type. This is primarily due to the fact that the behavior at the barrier interface is different resulting in different combinations and magnitude of incident, reflected and refracted stress waves. Results show that the reflected waves at a rigid barrier are of almost of the same magnitude as the incident waves. Reflected waves at a deformable barrier on the other hand, are of a magnitude that is substantially less than the incident waves. This may be explained by the fact that stresses, loads and energy generated at a rigid barrier are much higher than at a comparable deformable barrier. However, results also show that this early phase of wave propagation has very little effect on the final deformation (crush) pattern since the full duration of the impact is of several thousands wave reflections and refraction. This implies that in the real world conditions, the stress wave propagation along the rail has very little effect on the final deformed shape of the rail in a barrier impact.

## REFERENCES

1. Wagner,U.; Annandale,R.; Wüstner,H.; and Winkelmuller," A finite element model of the frontal deformable barrier as an example of simulating advanced requirements",SAE967123
2. McKellip, S.; Morschheuser, K.," Comparison between the FE crash analysis of a heavy class truck and two crash tests", SAE 947130
3. Zaouk, A., Bedewi, A., Kan, A., and Marzougui, D.)Validation of a Non-linear Finite Element Vehicle Model using Multiple Impact Data, presented and published in the International ASME Winter Annual Congress and exposition, Atlanta GA, November 17-22, © ASME 1996
4. Langner, W," The ODB test, a challenge to vehicle construction", SAE 967031
5. Cook et al., "Concepts and Applications of Finite Element Analysis", John Wiley & Sons, 1989
6. Xiao Lin, "Numerical Computation of Stress Waves in Solids", John Wiley & Sons, 1996.
7. Den Hartog, "Advanced Strength of Materials", pp 193, Dover, 1987.
8. X. Lin and J. Ballmann, "A Riemann solver and second-order Godunov's method for elastic-plastic wave propagation in solids", International Journal of Impact Engineering, 1993.

Figure 1. Model for type-1 rail

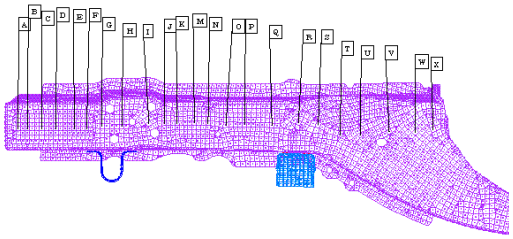

Figure 2. Model for type-2 rail

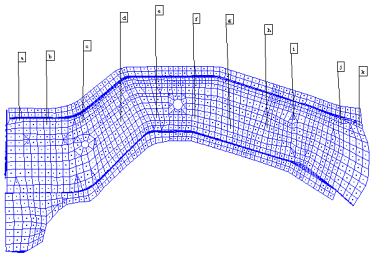

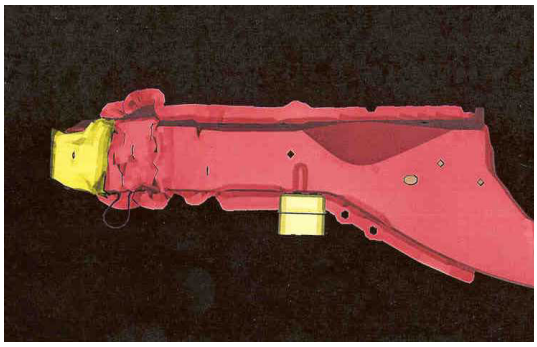

Figure 3. Deformed type-1 rail in Rigid barrier

Figure 4. Deformed type-2 rail in Rigid barrier

Figure 5.A Deformed type-1 rail in Deformable barrier

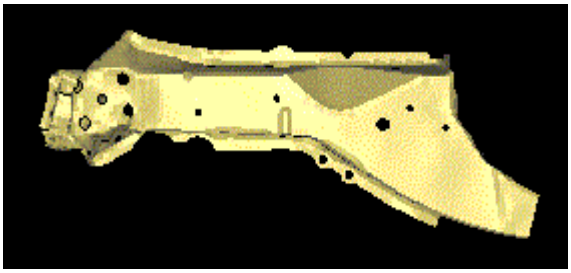

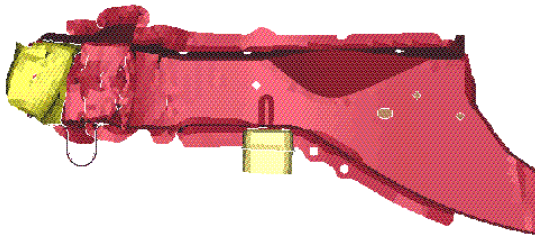

Figure 5-B Static deformed shape for type – 1 rail

Figure 6 Deformed type-2 rail in Deformable barrier

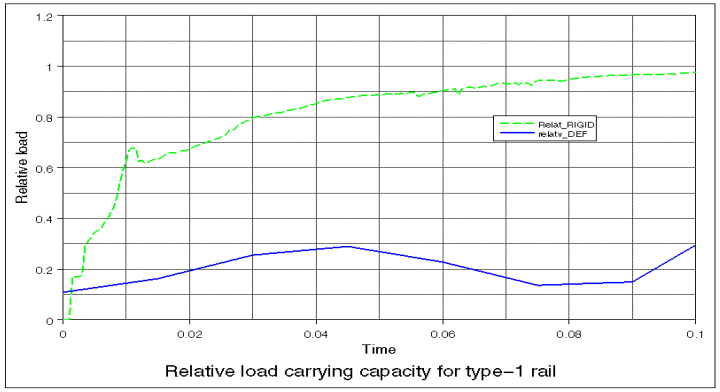


**Figure 7 Comparison of load of type-1 rail**

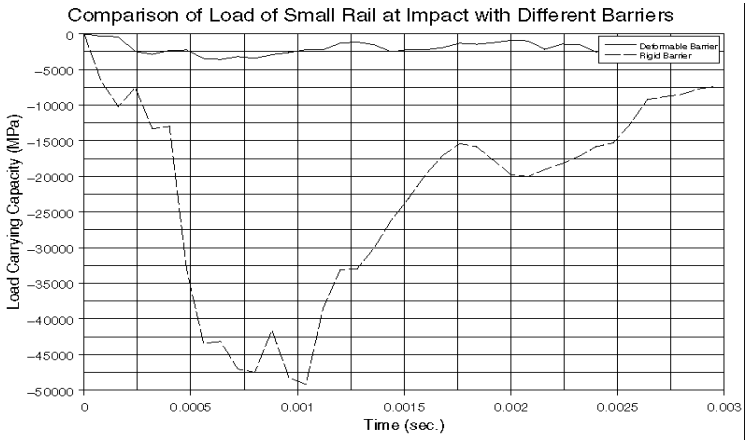


**Figure 8 Comparison of load of type-2 rail**

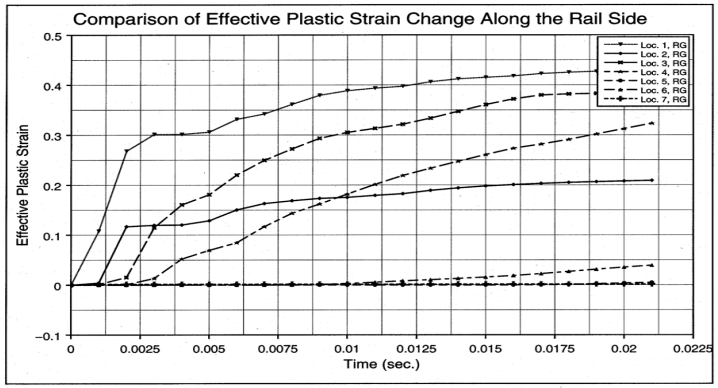


**Figure 9**

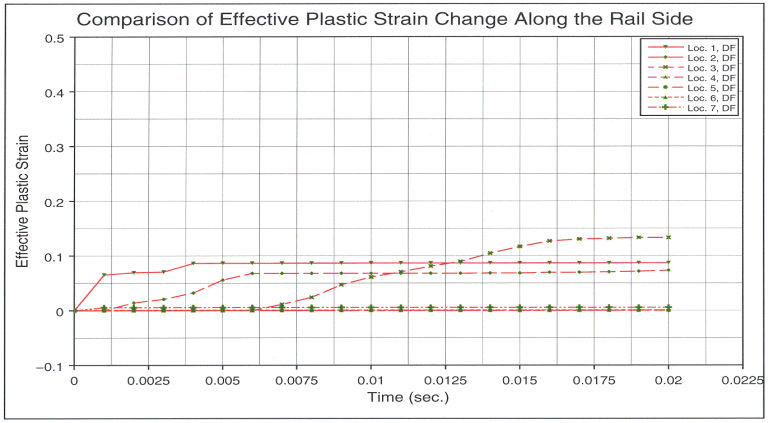


**Figure 10**

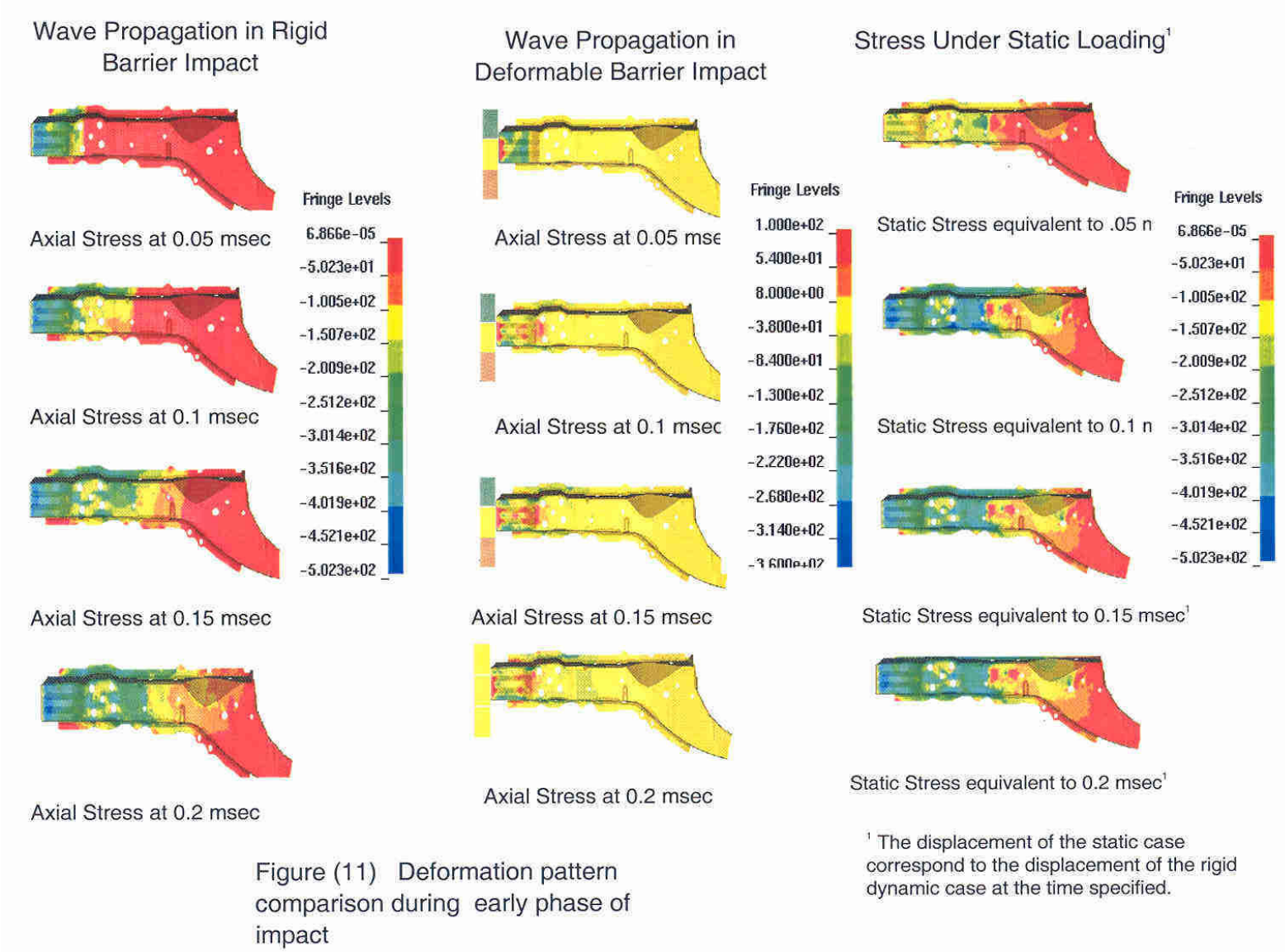


Figure (11) Deformation pattern comparison during early phase of impact

[1] The displacement of the static case correspond to the displacement of the rigid dynamic case at the time specified.

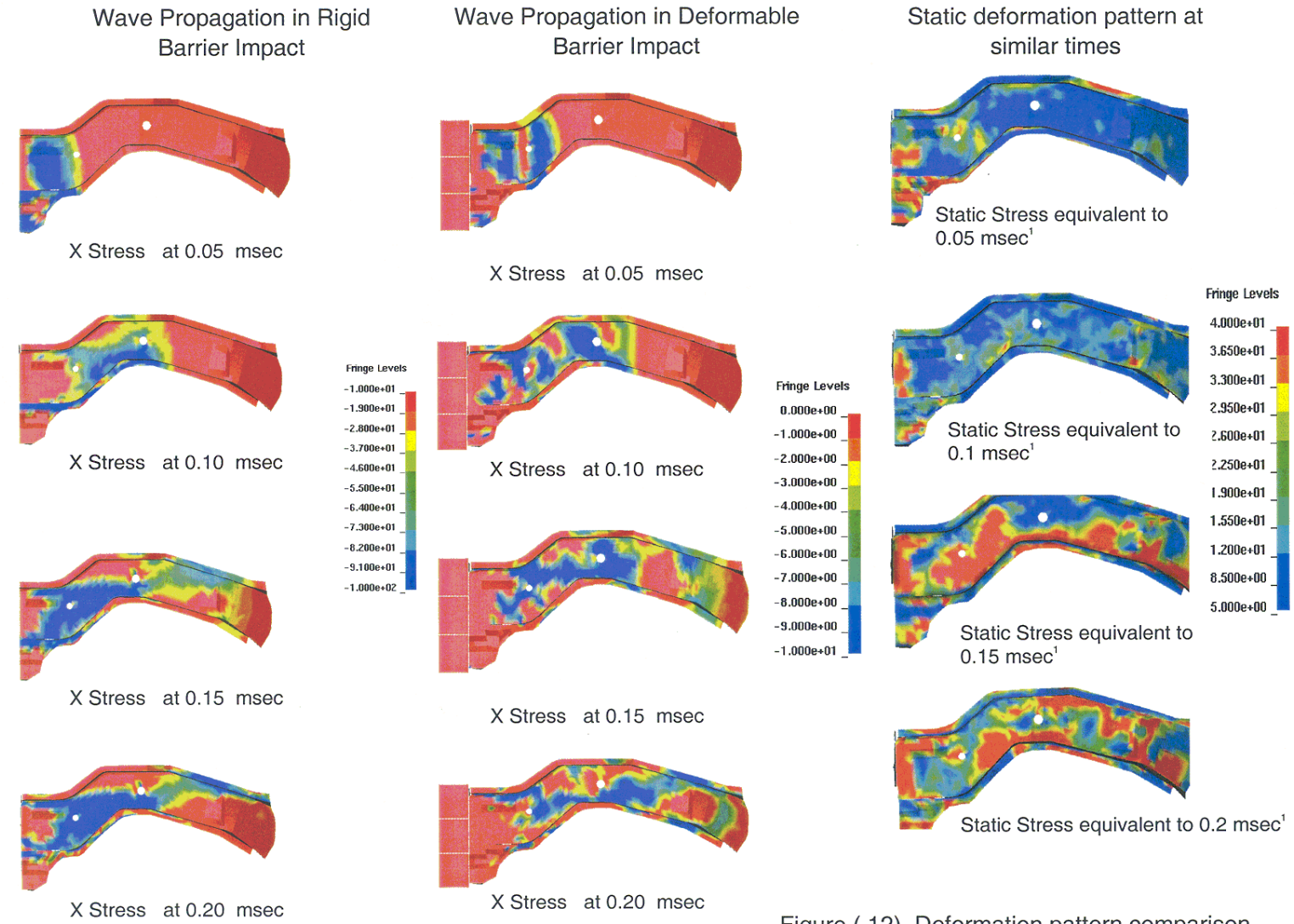


Figure ( 12) Deformation pattern comparison during initial phase of impact for Type-2 rail

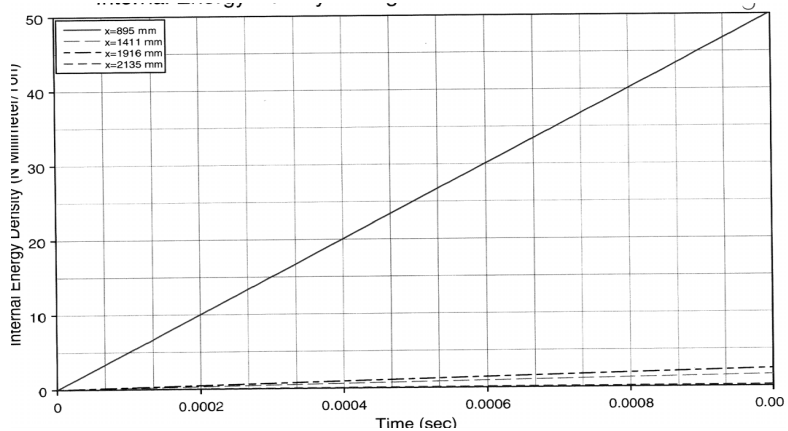


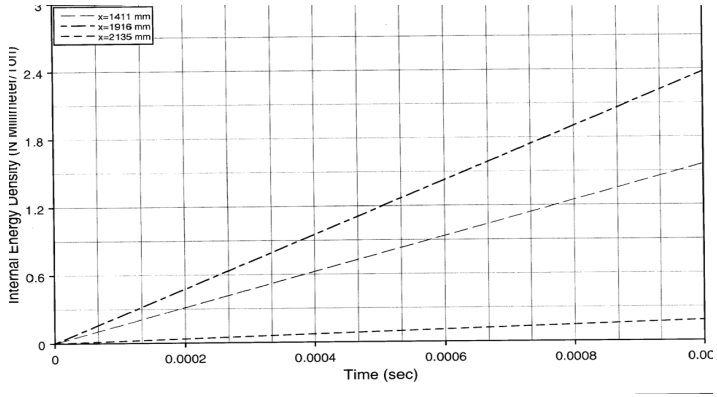


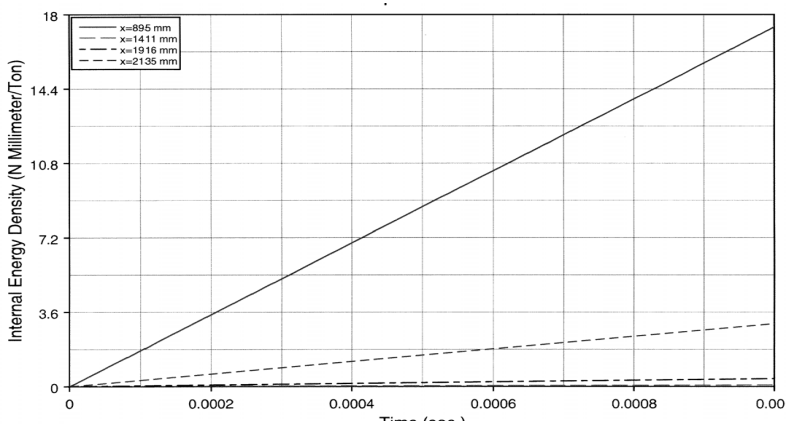


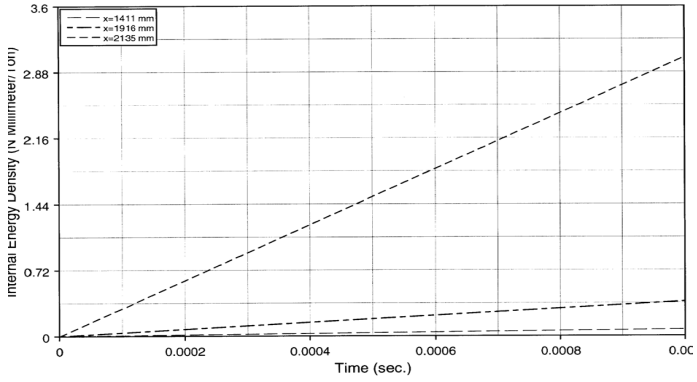


**Figure 13 Internal Energy Density perturbation for type-1 Rail**

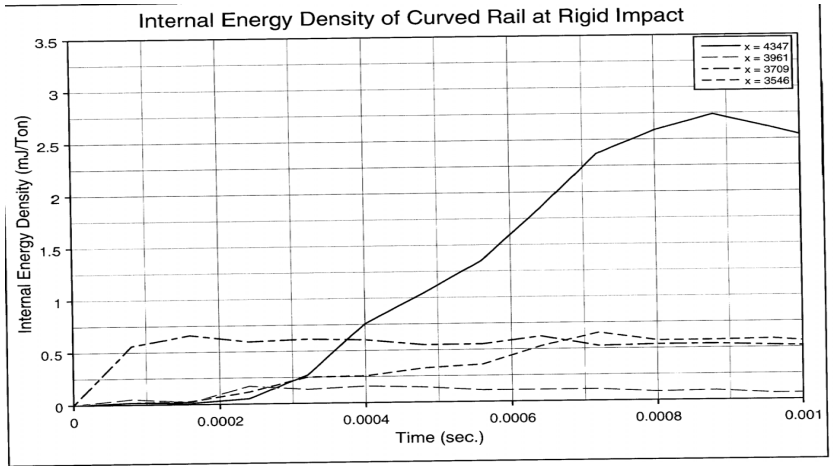


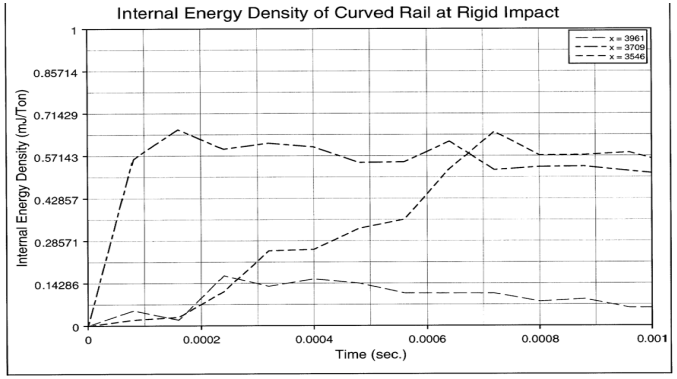


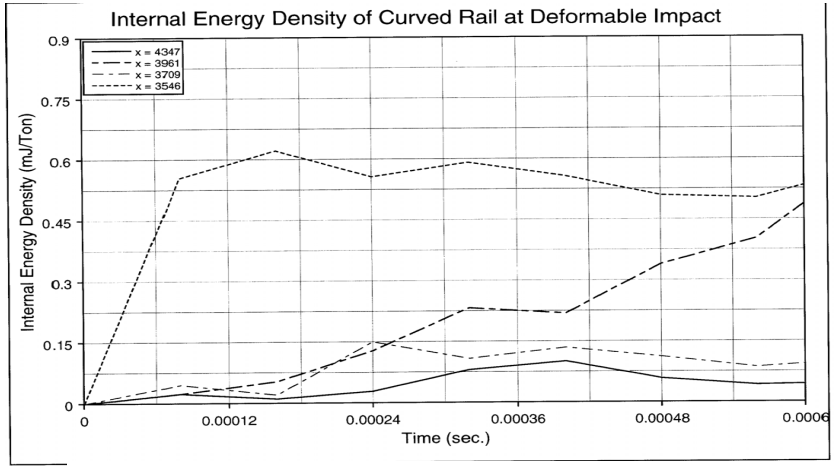


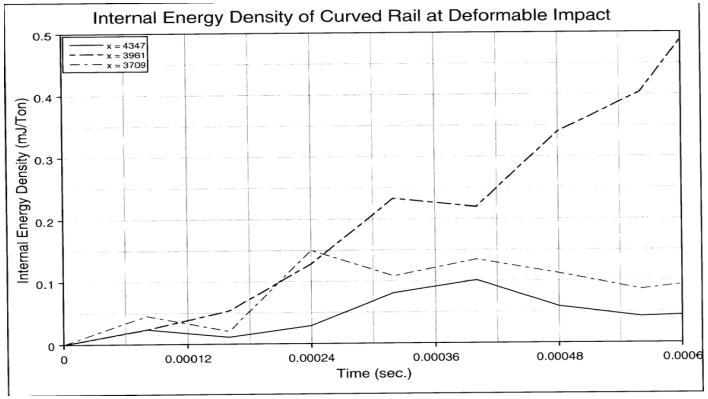


**Figure 14 Internal Energy Density perturbation for type-2 Rail**

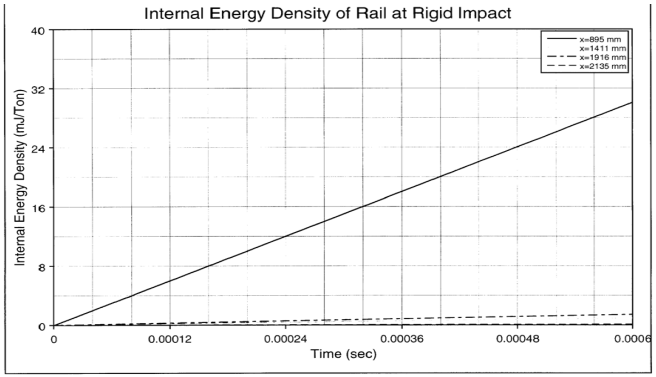


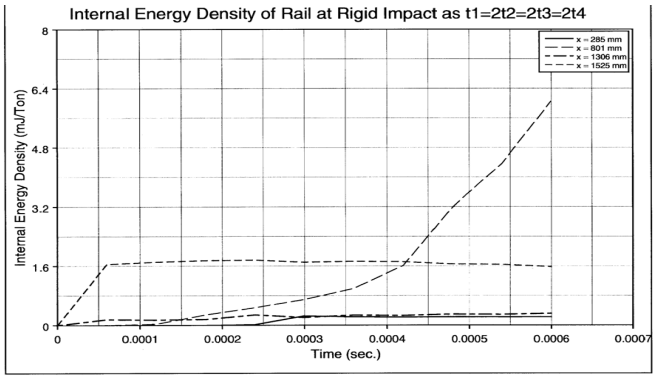


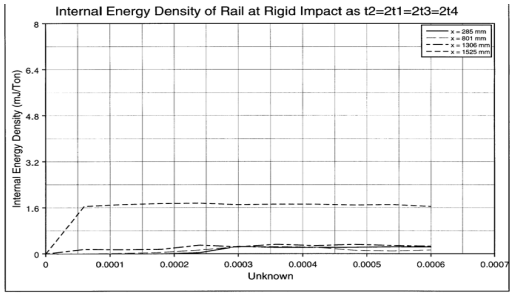


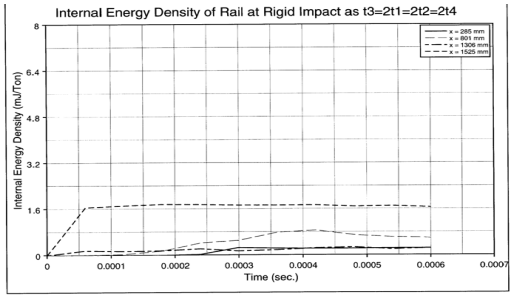


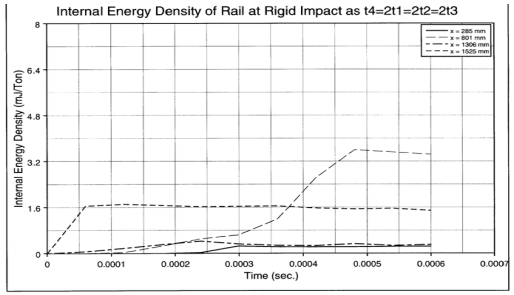


**Figure 15. Internal Energy Density of type-1 Rail in rigid impact with thickness change**

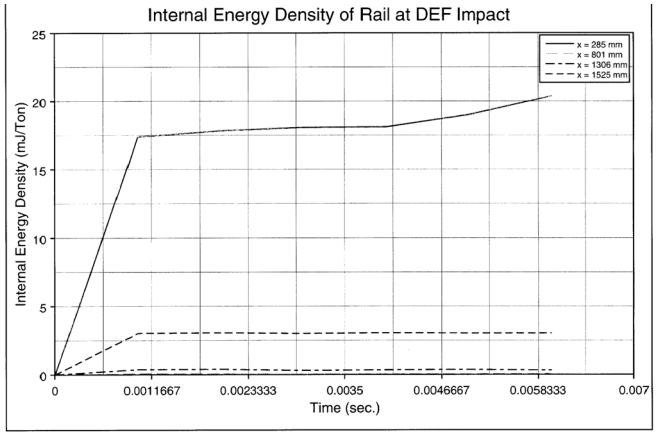


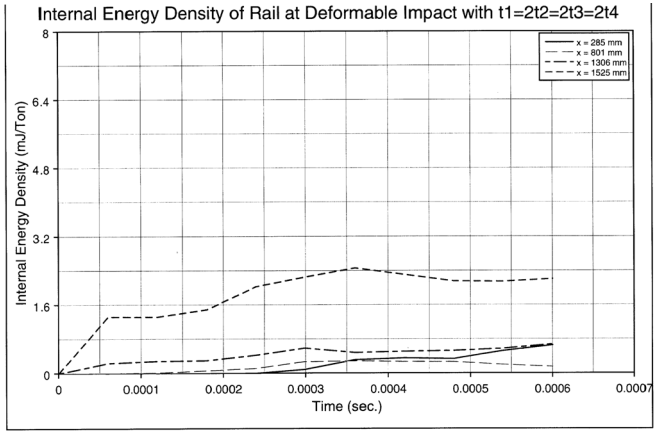


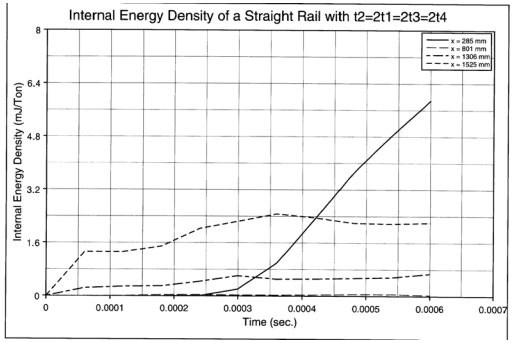


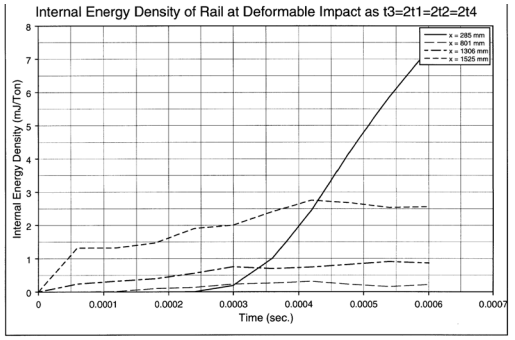


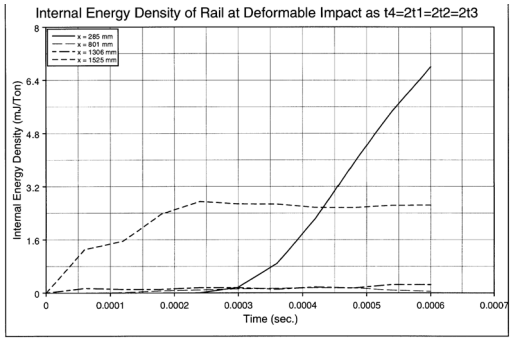


**Figure 16. Internal Energy Density of type-1 Rail in deformable impact with thickness change**

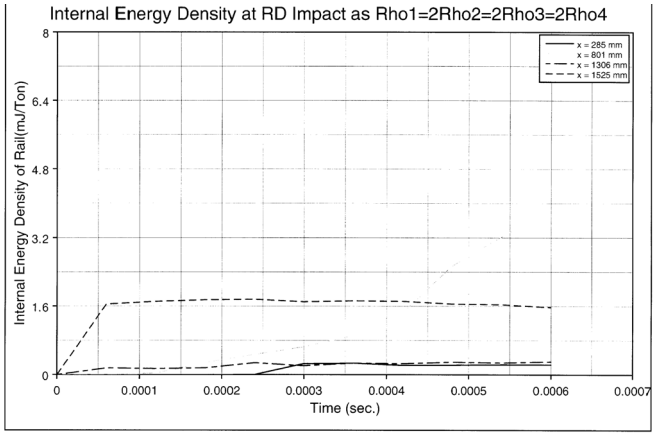


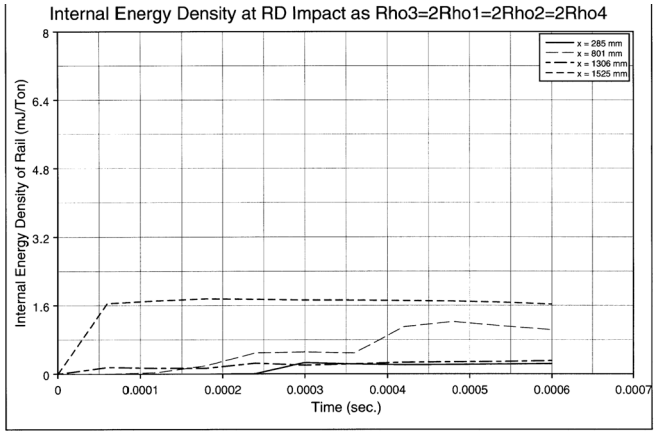


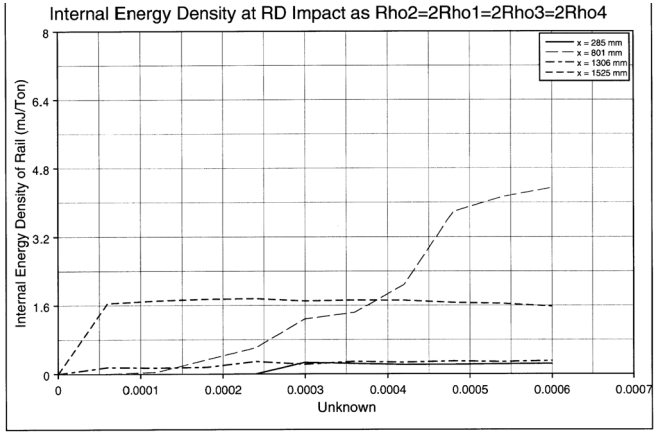


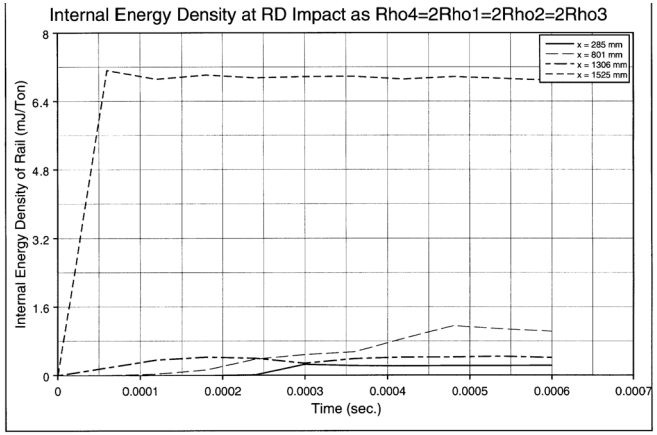


**Figure 17 A Internal Energy Density of type-1 Rail in rigid impact with density change**

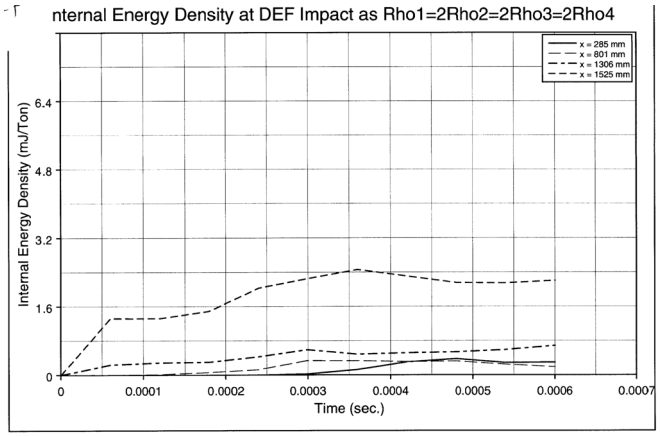


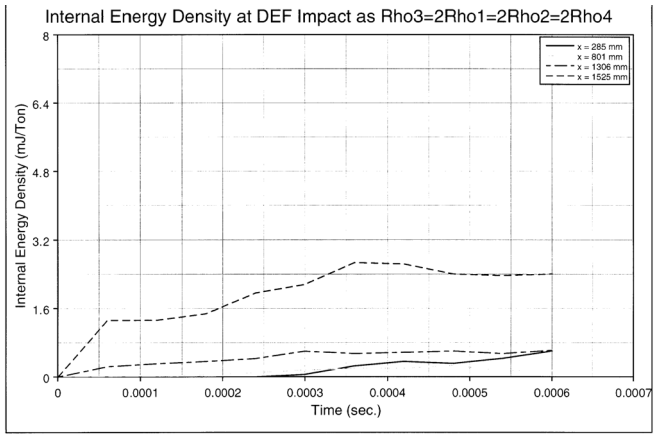


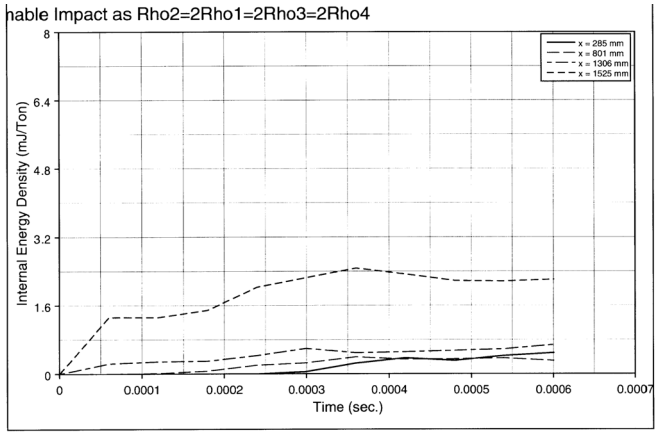


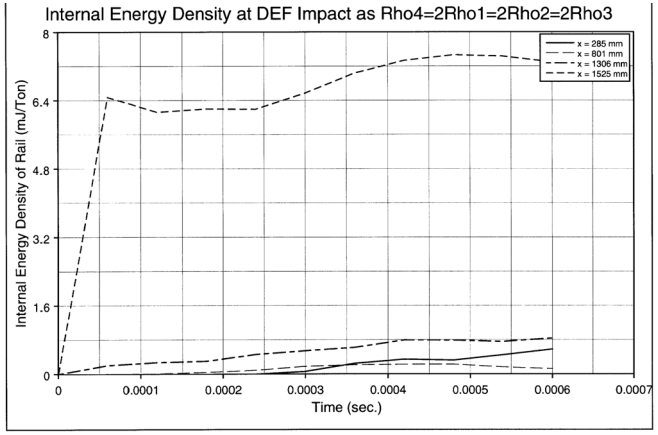


**Figure 18 Internal Energy Density of type-1 Rail in deformable impact with density change**

## List of Captions:

Figure 1 FE model for type –1 rail

Figure 2 FE model for type –2 rail

Figure 3 Deformed type-1 rail in rigid barrier impact

Figure 4 Deformed type-1 rail in deformable barrier impact

Figure 5 Deformed type-2 rail in rigid barrier impact

Figure 6 Deformed type-2 rail in deformable barrier impact

Figure 7 Comparison of load carrying capacity of type-1 rail

Figure 8 Comparison of load carrying capacity of type-2 rail

Figure 9 Comparison of plastic strain change in rigid impact along tail side for type-1 rail

Figure 10 Comparison of plastic strain change in deformable impact along tail side for type-1 rail

Figure 11 Deformation pattern comparison in early phase of impact for type-1 rail

Figure 12 Deformation pattern comparison in early phase of impact for type-2 rail

Figure 13
A Internal Energy Density Change of Type-1Rail with Time at Four Locations at Rigid Impact.
B Internal Energy Density Change of Type-1Rail with Time at Four Locations at Deformable Impact
C Internal Energy Density Change of Type-1Rail with Time at Three Locations at Rigid Impact
D Internal Energy Density Change of Type-1Rail with Time at Three Locations at Deformable Impact

Figure 14
A Internal Energy Density Change of Type-2 Rail with Time at Four Locations at Rigid Impact.
B Internal Energy Density Change of Type-2 Rail with Time at Four Locations at Deformable Impact
C Internal Energy Density Change of Type-2 Rail with Time at Three Locations at Rigid Impact.
D Internal Energy Density Change of Type-2 Rail with Time at Three Locations at Deformable Impact.

Figure 15
A Internal Energy Density of a Type-1Rail in rigid impact with t1=t2=t3=t4.
B Internal Energy Density of a Type-1Rail in rigid impact with t1=2t2=2t3=2t4.
C Internal Energy Density of a Type-1Rail in rigid impact with t2=2t1=2t3=2t4.
D Internal Energy Density of a Type-1Rail in rigid impact with t3=2t1=2t2=2t4.
E Internal Energy Density of a Type-1Rail in rigid impact with t4=2t1=2t2=2t3.

Figure 16
A Internal Energy Density of a Type-1Rail in deformable impact with t1=t2=t3=t4.
B Internal Energy Density of a Type-1Rail in deformable impact with t1=2t2=2t3=2t4.
C Internal Energy Density of a Type-1Rail in deformable impact with t2=2t1=2t3=2t4.
D Internal Energy Density of a Type-1Rail in deformable impact with t3=2t1=2t2=2t4.
E Internal Energy Density of a Type-1Rail in deformable impact with t4=2t1=2t2=2t3.

Figure 17
A Internal Energy Density of a Type-1Rail in rigid impact with Ro1=2Ro2=2Ro3=2Ro4.
B Internal Energy Density of a Type-1Rail in rigid impact with Ro2=2Ro1=2Ro3=2Ro4.
C Internal Energy Density of a Type-1Rail in rigid impact with Ro3=2Ro1=2Ro2=2Ro4.
D Internal Energy Density of a Type-1Rail in rigid impact with Ro4=2Ro1=2Ro2=2Ro3.

Figure 18
A Internal Energy Density of a Type-1Rail in deformable impact with Ro1=2Ro2=2Ro3=2Ro4.
B Internal Energy Density of a Type-1Rail in deformable impact with Ro2=2Ro1=2Ro3=2Ro4.
C Internal Energy Density of a Type-1Rail in deformable impact with Ro3=2Ro1=2Ro2=2Ro4.
D Internal Energy Density of a Type-1Rail in deformable impact with Ro4=2Ro1=2Ro2=2Ro3.